Materials Advances

Accepted Manuscript

This article can be cited before page numbers have been issued, to do this please use: O. V. Pylypova, K. Paliienko, A. Topchylo, A. Zaderko, V. Lysenko and V. A. Skryshevsky, *Mater. Adv.*, 2026, DOI: 10.1039/D6MA00445H.

ROYAL SOCIETY OF CHEMISTRY

rsc.li/materials-advances

Dynamic light scattering for probing metal ion induced aggregation of carbon dots

O. Pylypova[1, 2*], K. Paliienko[2, 3], A. Topchylo[2, 3], A. Zaderko[3], V. Lysenko[3] and V. Skryshevsky[1,2]

View Article Online
DOI: 10.1039/D6MA00445H

[1] Institute of High Technologies, Taras Shevchenko National University of Kyiv, Ukraine

[2] Corporation Science Park, Taras Shevchenko University of Kyiv, Ukraine

[3] Université Lyon 1, CNRS, Institut Lumière Matière, UMR5306, F-69100, Villeurbanne, France

**E-mail; olha.pylypova@knu.ua*

Abstract

Aggregate behaviour of carbon dots (CDs) in aqueous solutions in the presence of various metal ions was studied by means of dynamic light scattering (DLS). Colloidal CDs with different surface chemistries were exposed to Cu^{2+}, Pb^{2+}, Fe^{3+}, Gd^{3+}, and Ag^{+} ions at micromolar concentrations. The DLS measurements revealed a pronounced increase in hydrodynamic size upon metal ion addition, indicating the formation of metal-mediated CDs agglomerates. A distinct saturation of aggregate size values is observed, suggesting a finite number of accessible coordination sites on the CDs surface. To quantitatively compare ion-specific effects, an empirical aggregation ion efficiency parameter (IAE), defined as the ratio of the saturation aggregate size to the corresponding saturation ion concentration, is introduced. The IAE parameter strongly depends on the nature of the metal ion and does not directly correlate with its charge state. The presented experimental approach demonstrates that DLS-based aggregation analysis provides valuable structural insight into metal-CD interactions and complements optical sensing techniques for the development of advanced nanoanalytical strategies for heavy metal detection.

Keywords: carbon dots, metal ions, dynamic light scattering, aggregation efficiency, chelating agents

Heavy metal ions are among the most hazardous environmental pollutants due to their toxicity, non-biodegradability, and tendency to accumulate in living organisms. These metal ions are widely distributed in agricultural systems, soils, natural waters, and industrial wastewater as a result of intensive industrialization and anthropogenic activities. Heavy metal contamination poses a serious threat to human health and ecosystems, as even trace concentrations can cause significant toxic effects.[1] Exposure to heavy metals such as Cu^{2+}, Pb^{2+}, Fe^{3+}, Ag^{+}, and Gd^{3+} has been linked to severe adverse health effects, including neurological disorders, renal dysfunction, cardiovascular diseases, and carcinogenicity. Lead (Pb^{2+}) is a well-known neurotoxin that affects cognitive development, particularly in children, even at very low concentrations.[2] Copper (Cu^{2+}), although an essential trace element, becomes toxic at elevated levels, causing oxidative stress and liver damage.[3] Excess iron (Fe^{3+}) can catalyze the formation of reactive oxygen species, leading to cellular damage and neurodegenerative diseases.[4] Disturbances in the balance between Fe^{3+} and Fe^{2+} ions can have serious

consequences for human health, as these ions are involved in a wide range of biological processes, including oxygen transport, cellular metabolism, and enzymatic reactions[5]. Silver ions (Ag^+) exhibit antimicrobial activity but may induce argyria and cytotoxic effects upon chronic exposure.[4] Gadolinium-based compounds, widely used as contrast agents in magnetic resonance imaging (MRI), have raised concerns due to their potential deposition in tissues and associated toxicity.[6] Given the stringent regulatory limits imposed by organizations such as the World Health Organization (WHO) and the U.S. Environmental Protection Agency (EPA), sensitive and reliable methods for monitoring heavy metal ions in aqueous environments are critically needed.

A variety of analytical techniques have been developed for the detection of heavy metal ions in liquids. Atomic absorption spectroscopy (AAS) and inductively coupled plasma mass spectrometry (ICP-MS) are widely used due to their high sensitivity and accuracy.[7] However, these techniques typically require expensive instrumentation, skilled personnel, and complex sample preparation, which limits their applicability for on-site or real-time analysis. Electrochemical methods, including anodic stripping voltammetry, offer relatively low detection limits and portability;[8] nevertheless, they often suffer from electrode fouling, matrix interferences, and limited selectivity in complex samples. Colorimetric and spectrophotometric methods are simple and cost-effective but generally exhibit lower sensitivity and reduced selectivity, particularly at trace concentration levels.[9] Overall, while conventional methods provide excellent analytical performance under laboratory conditions, their inherent limitations motivate the development of alternative nanoanalytical approaches that are simple, rapid, cost-effective, and suitable for in situ detection.

Carbon dots (CDs) are nanoscale carbon-based materials composed of carbonaceous cores functionalized with various surface groups, including hydroxyl, carboxyl, and amino groups.[10] Particular interest in CDs arises from their unique optical and electronic properties, such as high quantum yield, photostability, physicochemical stability, and the ability to tailor their characteristics through particle size control and surface functionalization.[11] Owing to these properties, CDs have been extensively investigated for applications in photocatalysis.[12], as antibacterial agenti[13], and in bioimaging and theranostics.[14] Furthermore, CDs have emerged as versatile nanomaterials for metal ion sensing owing to their strong photoluminescence, water solubility, low toxicity, and tunable surface chemistry [15-17] Interactions between surface functional groups and metal ions induce changes in fluorescence intensity, wavelength, or lifetime, enabling sensitive optical detection. The presence of Cu^{2+} inducing fluorescence quenching via photoinduced electron transfer or coordination-mediated aggregation, with detection limits in the nM–μM range.[18,19] CDs have also demonstrated high sensitivity toward Pb^{2+} and Fe^{3+} ions, often achieving nM-level detection limits through fluorescence quenching or aggregation-related effects.[20-23]Ag^+ sensing has been reported with detection limits in the tens of nM, depending on CD surface chemistry.[24,25]

View Article Online
DOI: 10.1039/D6MA00445H

Despite extensive research on luminescence-based sensing, most studies involving CDs are exclusively focused on optical signal changes, while structural transformations such as aggregation are often overlooked. The increasing complexity of environmental and biological samples demands analytical techniques that provide both chemical sensitivity and structural information. Luminescence based methods, while powerful, often lack insight into the physical processes governing nanoparticle-ion interactions. Therefore, the development of new diagnostic strategies integrating optical and analytical techniques is essential for advancing heavy metal ion detection and for the rational design of next generation sensing platforms.

Dynamic Light Scattering (DLS) is a non-invasive optical technique used to study size and aggregation behaviour of nano- and micro-scale particles in dispersion.[26,27] The method is based on the analysis of temporal fluctuations of scattered laser light caused by the Brownian motion of particles. From the autocorrelation function of the scattered intensity, the translational diffusion coefficient is determined and converted into the hydrodynamic diameter using the Stokes–Einstein equation. Since larger particles diffuse more slowly than smaller ones, the decay rate of the correlation function directly reflects changes in particle size. The formation of agglomerates leads to a significant change in the DLS signal. Because the scattering intensity (I) strongly depends on particle size (d) as flowing: $I \sim d^6$, even a small number of aggregates dominates the scattering response. As individual nanoparticles form agglomerates, the intensity fluctuations become slower and their average amplitude increases. Thus, monitoring the evolution of scattering intensity and size distributions allows DLS to effectively track the agglomeration process, for example, during the interaction of CDs with metal ions.

While the use of CDs for metal ion sensing is already well established, the novelty of the present work lies in the DLS-based analysis of the CDs aggregation and saturation induced by metal ions. Specifically, how the size of the aggregates changes when metal ions are added to the colloidal solution of CDs. In particular, we examine what factors they depend on: nature of the ions, their charge number and minimum concentration of metals.

CDs were synthesized by solvothermal carbonization of a mixture of urea and anhydrous citric acid.[28] In a typical procedure, 10 g of urea (p.a., Sigma, 0.167 mol) and 16 g of anhydrous citric acid (Sigma, pharmaceutical grade, 0.083 mol) were thoroughly mixed in a mortar until a homogeneous precursor mixture was obtained. The resulting mixture was transferred into an open glass reactor. The reactor was placed in a drying oven and heated from room temperature (25 °C) to 135 °C over 30 min, followed by thermal treatment at 135 °C for 2 h, resulting in the formation of a yellow molten phase. Subsequently, the temperature was increased to 165 °C within 10 min and maintained for an additional 1 h. During this stage, the reaction mixture gradually transformed into a dark brown shiny solid product.

View Article Online
DOI: 10.1039/D6MA00445H

After completion of the thermal treatment, 75 mL of an ethanol/water mixture (15:85 v/v) was added to dissolve the obtained solid material. The resulting dark brown dispersion was filtered through Gossypium album in order to remove coarse insoluble carbonized by-products. The filtrate was then acidified by addition of 20 mL of glacial acetic acid. Upon acidification, the carbon dots formed visible flocculates in the solution. The suspension was allowed to stand for 24 h, after which the precipitated product was collected by vacuum filtration and dried in air to obtain a brown powder of CDs.

Detailed description of the synthesis and main physico-chemical characteristics of the CDs are provided in our previous works.[28] CDs consist of a graphene-like core and their surface chemistry is represented by the following bonds: -COOH, -C=O and -CO-O-, -N-H, -O-H.[22] Schematic illustration of the CDs is shown in Figure 1

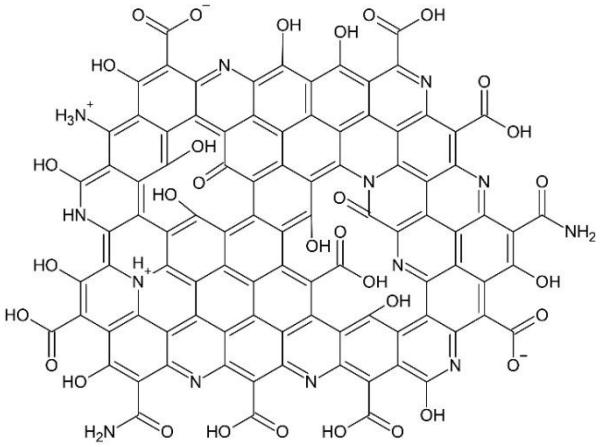

Fig. 1. Schematic illustration of chemical structures of the synthesized CDs samples

For preparation of stock dispersions, the synthesized CDs powder was dissolved in deionized water with addition of sodium bicarbonate (p.a., Fisher Scientific) until complete dissolution was achieved, resulting in a final CDs concentration of 1 g/L. Sodium bicarbonate was used to partially neutralize carboxylic acid groups present on the surface of the CDs, improving their dispersibility in aqueous media and stabilizing the colloidal system. Under these conditions, the resulting dispersion exhibited a pH value of 6.7 without further adjustment.

This stock dispersion was subsequently diluted 256-fold with deionized water to obtain the working CDs solutions used for DLS measurements and metal ion addition experiments.

All metal ions were introduced in the form of nitrate salts. Fresh 0.01 M stock solutions of the corresponding metal nitrates were prepared in deionized water (18 MOhm) immediately before use and subsequently diluted to the required micromolar concentrations for aggregation experiments.

Size distribution measurements were performed by means of DLS with the use of ZetaSizer Nano S equipment (Malvern Instruments, U.K.). Aqueous colloidal solutions of CDs (4 mg/L, pH 6.7) with 0-16 μM of Me^{n+}) were illuminated by He-Ne laser (632.8 nm) and the scattered light was

View Article Online
DOI: 10.1039/D6MA00445H

detected at 173°. For statistics and to ensure reproducibility of the experiments, all the DLS measurements were carried out 10 times with 10 repetitions for each measurement.

Figure 2 presents size distributions of CDs colloids measured by DLS as a function of Gd^{3+} (Fig. 2a) and Fe^{3+} (Fig. 2b) concentrations at pH 6.7. In the absence of the metal ions, CDs exhibit a narrow hydrodynamic size distribution in the range of 1–10 nm, corresponding to well-dispersed individual carbon dots. Upon gradual addition of Gd^{3+} or Fe^{3+} ions, the size distributions shift monotonically toward larger hydrodynamic diameters, indicating the formation of metal ion induced agglomerates of CDs. This behaviour reflects the role of positively charged metal ions as coordination centers that bridge negatively charged surface functional groups of CDs.

As the metal ion concentration increases, the agglomerate size approaches a saturation value. For Gd^{3+} ions, saturation of the aggregate size is achieved at metal concentrations ~3 μM, yielding agglomerates with characteristic hydrodynamic diameters of 40–50 nm. In contrast, Fe^{3+} ions require significantly higher concentrations (~9 μM) to reach the saturation of aggregate size, resulting in much larger aggregates with diameters up to ~80 nm. This difference indicates a stronger and more efficient interaction of Gd^{3+} ions with the surface functional groups of CDs compared to Fe^{3+} ions.

The inset in Fig. 2a shows an evolution of Z-potentials of CDs-based colloids as function of Gd^{3+} concentration. The Z-potential decreases progressively and approaches zero at ~5.8 μM of Gd^{3+}, confirming compensation of initial negative surface charge of colloidal CDs by positive charges of the metal ions.

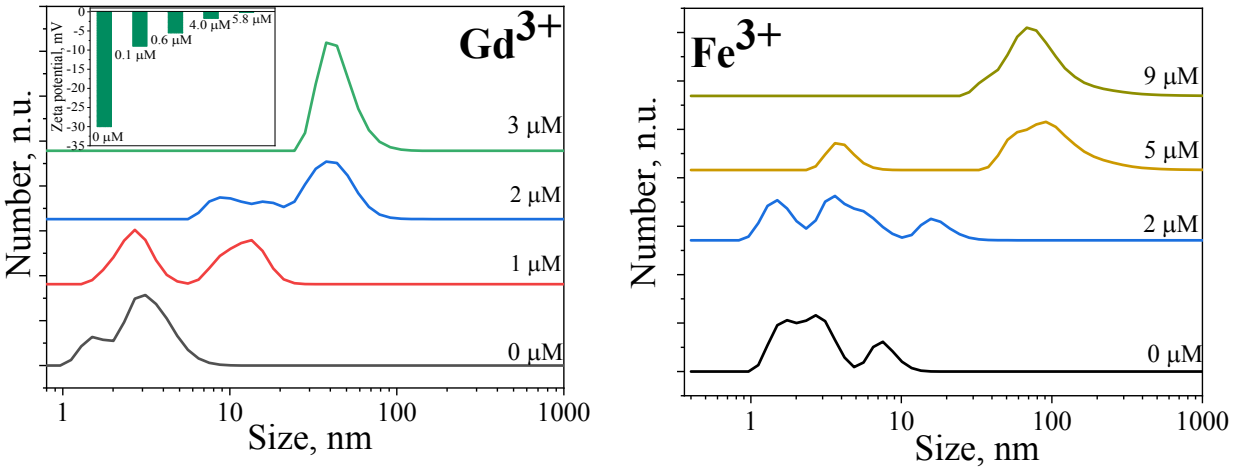

(a) **(b)**

Fig. 2. Size distribution of CDs depending on concentrations of ion metals: a) Gd^{3+} and b) Fe^{3+}, pH 6.7. In insert: Zeta potential of CDs depending on concentrations of Gd^{3+}-ions.

Figure 3 shows the aggregation behaviour of CDs in presence of Pb^{2+} ions. Initial hydrodynamic size distributions without metal ions are the similar (1–10 nm) to those shown in Fig. 2. Increasing Pb^{2+} concentration induces aggregation in CDs colloids. However, saturation in this case is reached at higher ion concentrations being around 16 μM. Impact of the same ion type on

another type of CDs synthesized from coffee wastes is shown in Fig. S1(see Supplementary Information section). Globally, the same agglomeration effect takes place for any kind of CDs, but agglomeration dynamics and final aggregate size depend on chemical composition of CDs.

View Article Online
DOI: 10.1039/D6MA00445H

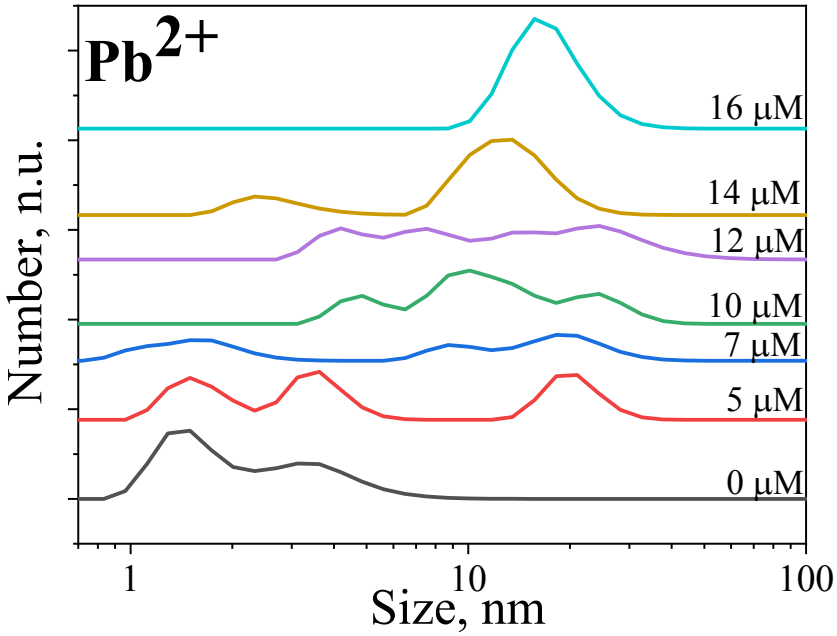

Fig. 3. Size distributions of CDs depending on concentrations of Pb^{2+} ions

Figure 4 summarizes the maximum hydrodynamic sizes of CDs aggregates induced by different metal ions (Cu^{2+}, Ag^{+}, Gd^{3+}, Fe^{3+}, Pb^{2+}) as function of the minimum ion concentration required to reach the saturation of aggregate sizes. The saturation state is achieved at relatively low concentrations for Cu^{2+} (~1 μM), Ag^{+} (~3 μM), and Gd^{3+} (~3 μM). In contrast, significantly higher concentrations are required for Fe^{3+} (~9 μM) and Pb^{2+} (~16 μM). Cu^{2+} ions exhibit the highest aggregation efficiency, inducing compact aggregates with characteristic sizes of ~16 nm at the lowest concentration. Although Pb^{2+} ions carry the same charge, it requires an order of magnitude higher concentration to induce a similar degree of aggregation, highlighting the importance of ion-specific coordination chemistry. Fe^{3+} ions are the least efficient, forming the largest aggregates (~80 nm) only at relatively high concentrations. Gd^{3+} ions show intermediate behaviour, yielding aggregates of moderate size (~40 nm).

View Article Online
DOI: 10.1039/D6MA00445H

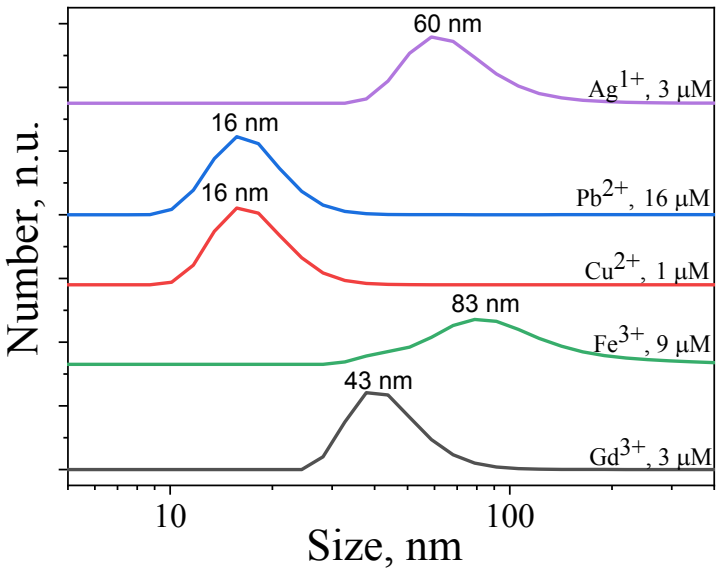

Fig. 4. Saturated size distributions of CDs aggregates induced by presence of the following metal ions: Gd^{3+}, Fe^{3+}, Pb^{2+}, Cu^{2+}, Ag^{1+} at their different minimal concentrations

The DLS results clearly demonstrate that metal ion induced aggregation of CDs is governed by coordination-mediated interactions rather than by purely electrostatic effects. Although electrostatic charge compensation contributes to the initial destabilization of the colloidal system, the observed ion-specific aggregation behaviour cannot be explained solely by ionic charge. Instead, the aggregation efficiency is controlled by a combination of factors, including metal–ligand coordination strength, hydration energy, and steric constraints. Positively charged metal ions interact with oxygen- and nitrogen-containing functional groups on the CD surface (–COO–, –OH, –C=O, –NH–), forming interparticle coordination bridges that link individual CDs into larger agglomerates.[15,16,29]

The absence of a direct correlation between ionic charge and aggregation efficiency is particularly evident when comparing Cu^{2+} and Pb^{2+} ions. Despite identical charge states, Cu^{2+} induces aggregation at significantly lower concentrations than Pb^{2+}, indicating stronger coordination affinity toward CD surface ligands. Similar conclusions have been reported for CD-based metal sensing systems, where ion selectivity is governed by coordination chemistry rather than electrostatics alone.[30,35]

Hydration effects play a central role in this process. In aqueous media, metal ions are surrounded by hydration shells that shield their charge and hinder direct coordination with surface ligands. Formation of CD-metal-CD bridges require partial dehydration of the ion and replacement of water molecules by surface functional groups. Highly hydrated ions such as Fe^{3+} and Gd^{3+} exhibit higher dehydration energies, shifting aggregation to higher ion concentrations.[36-38] In contrast, moderately hydrated ions such as Cu^{2+} more readily undergo partial dehydration, enabling efficient bridge formation at low concentrations.

View Article Online
DOI: 10.1039/D6MA00445H

Steric effects further limit aggregate growth and lead to the observed saturation behaviour.[39] As agglomerates grow, surface-bound functional groups and hydrated metal complexes create steric barriers that hinder further approach of additional CDs. Once available coordination sites become shielded, further aggregation becomes energetically unfavourable, resulting in a stable saturation size detectable by DLS.[26] As aggregation proceeds, steric hindrance arising from the finite size of the carbon dots, surface functional groups, and hydrated metal complexes limits further growth of the agglomerates. This steric stabilization ultimately leads to a saturation of the hydrodynamic size observed by DLS. Schematic aggregation mechanism is presented in Fig. 5.

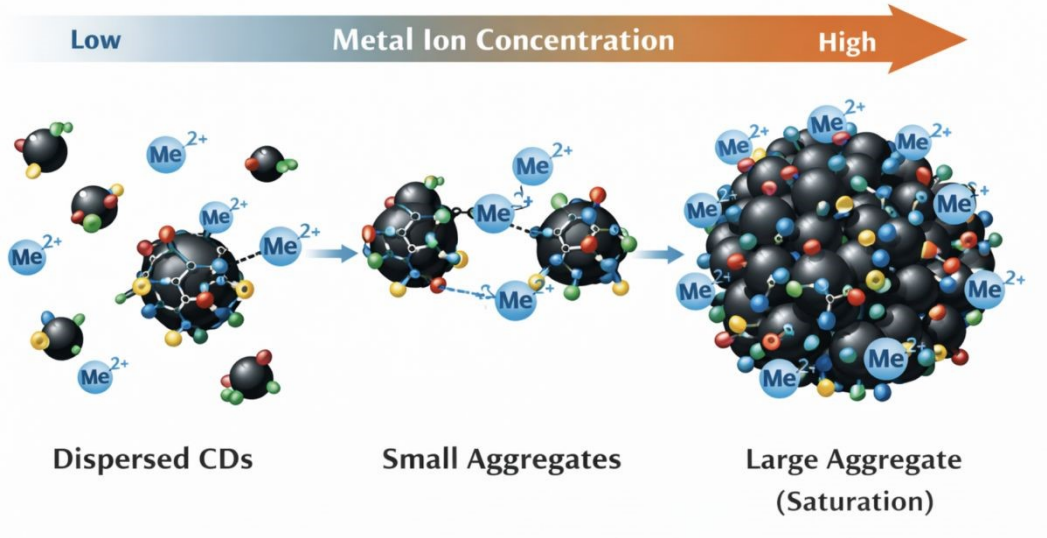

Fig 5. Schematic illustration of metal ion induced aggregation of CDs. Black spheres represent CD cores (sp^2/sp^3-hybridized carbon framework), while coloured surface moieties correspond to oxygen and nitrogen containing functional groups ($–COO^-$ / –COOH (red), –OH (green), $–NH_2$ / –NH– (yellow), C–O / C–N (Light blue (surface). Blue circles denote metal ions (Me^{2+}), which at intermediate concentrations act as coordination bridges between individual CDs, leading to cluster formation. At high metal ion concentrations, extensive cross-linking results in the formation of large CD-Me^{2+} globular aggregates, corresponding to the saturation regime observed by DLS.

To enable a quantitative comparison of the ability of different metal ions to induce carbon dot aggregation, an empirical Ion Aggregation Efficiency (IAE**)** parameter was introduced (Table 1). This parameter is defined as the ratio between the saturation hydrodynamic diameter of CD aggregates and the minimum metal ion concentration required to reach the saturation regime: $E_{\mathrm{ion}} = d_{\mathrm{sat}}/C_{\mathrm{sat}}$. Although this parameter is not a standard physicochemical quantity, it provides a convenient comparative metric for evaluating ion-specific aggregation behaviour under identical experimental conditions.

Table 1. Ion_Aggregation_Efficiency

Rank	Metal ion	Charge	C_sat (μM)	d_sat (nm)	E_ion (nm·μM⁻¹)
1	Cu^{2+}	+2	1	16	16.0
2	Gd^{3+}	+3	3	43	14.3
3	Fe^{3+}	+3	9	83	9.2
4	Ag^{+}	+1	3	20	6.7
5	Pb^{2+}	+2	16	16	1.0

As summarized in Table 1**,** the aggregation efficiency follows the order: $Cu^{2+} > Gd^{3+} > Fe^{3+} > Ag^{+} > Pb^{2+}$. This ranking does not correlate with the formal charge of the ions and clearly demonstrates that aggregation is governed by ion-specific coordination chemistry rather than by electrostatic interactions alone. In particular, Cu^{2+} ions exhibit the highest aggregation efficiency, inducing compact CD_1 aggregates at the lowest concentration (~1 μM). This behaviour is consistent with the well-documented strong affinity of Cu^{2+} toward oxygen- and nitrogen-containing ligands, which has been widely reported in CD-based sensing systems [30-32]. Despite having the same charge state as Cu^{2+}, Pb^{2+} ions show markedly lower aggregation efficiency, requiring concentrations an order of magnitude higher to reach saturation. The aggregation of CDs in the presence of Pb^{2+} ions is attributed to the coordination of Pb^{2+} with oxygen-containing surface functional groups, primarily carboxyl and hydroxyl groups. Upon binding, Pb^{2+} ions can act as interparticle linkers, connecting adjacent CDs through coordination bridges and thereby promoting cluster formation. As the Pb^{2+} concentration increases, the number of interparticle bridges grows, resulting in the formation of progressively larger aggregates until a saturation regime is reached. The relatively large ionic radius and lower charge density of Pb^{2+} reduce the efficiency of these coordination interactions, which explains why higher Pb^{2+} concentrations are required to induce extensive aggregation. This difference highlights the role of coordination geometry and ligand-field effects, which strongly influence the formation of interparticle metal-ligand bridges.

The behaviour of trivalent ions further supports this interpretation. Fe^{3+} ions exhibit relatively low aggregation efficiency and form the largest aggregates only at elevated concentrations. This can be attributed to their strong hydration shell and high dehydration energy, which hinder direct coordination with CD surface functional groups. Similar effects have been observed for Fe^{3+} in fluorescence-based CD sensors, where strong hydration limits binding efficiency despite high ionic charge.[33]

View Article Online
DOI: 10.1039/D6MA00445H

Gd^{3+} ions display intermediate aggregation efficiency, forming aggregates of moderate size at lower concentrations than Fe^{3+}. This behaviour is consistent with previous reports on lanthanide–carbon dot interactions, which demonstrate strong coordination tendencies accompanied by partial dehydration and structural reorganization of the nanoparticle system.[40] The present DLS results provide direct structural evidence for these coordination-induced aggregation processes. Ag^{+} ions show moderate aggregation efficiency, reflecting their weaker hydration but also reduced coordination strength toward oxygen-dominated ligands on the CD surface.[41,42] This balance results in limited aggregation efficiency compared to Cu^{2+}, despite the lower hydration barrier.

Overall, the analysis of Table 1, in combination with Figure 4**,** demonstrates that ion-induced aggregation of CD is controlled by a delicate interplay between metal-ligand coordination strength, hydration energy, and steric accessibility of surface functional groups. The IAE parameter therefore serves as a useful comparative descriptor for assessing metal-CD interactions and complements qualitative DLS observations.

In this work, metal ion induced aggregation of CDs in aqueous solutions was systematically investigated by means of DLS measurements. The results demonstrate that aggregation is driven by coordination-mediated interactions between metal ions and surface functional groups of CDs, rather than by simple electrostatic screening.

For all investigated metal ions (Cu^{2+}, Pb^{2+}, Fe^{3+}, Gd^{3+}, and Ag^{+}), a pronounced saturation of the hydrodynamic aggregate size was observed, indicating a finite number of accessible coordination sites on the CD surface. The saturation behaviour reflects the balance between metal-ligand coordination, ion hydration, and steric stabilization effects.

An empirical aggregation efficiency parameter was introduced to quantitatively compare ion-specific aggregation behaviour. This parameter revealed strong dependence on the chemical nature of the metal ion and no direct correlation with ionic charge. Cu^{2+} ions exhibited the highest aggregation efficiency, whereas Fe^{3+} and Pb^{2+} required significantly higher concentrations to induce comparable aggregation.

Conclusion

Overall, the presented DLS-based approach provides valuable structural insight into metal-CD interactions and complements conventional luminescence-based sensing techniques. The observed aggregation process can be interpreted as a surface-mediated chelation mechanism, in which heterogeneous functional groups on CDs act as multidentate coordination sites, enabling effective sequestration of metal ions into nanoscale aggregates. This understanding opens new perspectives for the rational design of CD-based sensing and remediation platforms. Upon partial dehydration, metal ions can form coordination bridges between adjacent CDs, resulting in the sequestration of metal ions within larger aggregates. Although this process differs from classical molecular chelation in terms of

structural definition and thermodynamic description, it shares several key features, including ion selectivity, multidentate binding, and the effective removal of metal ions from the aqueous phase.

View Article Online
DOI: 10.1039/D6MA00445H

Author Contributions

O.P., V.S., and V.L.- concept and analysis; O.P., A.T., K.P., A.Z. - investigation; O.P. - original draft preparation; V.L. and V.S.- supervision. The manuscript was written through contributions of all authors. All authors have given approval to the final version of the manuscript.

Conflicts of interest

The authors declare no competing financial interest.

Data availability

he main data supporting the findings of this study are provided within the article and its Supplementary Information (SI). The SI includes size distributions of carbon dots (CDs) synthesized from coffee waste as a function of Pb^{2+} ion concentration, as well as a schematic illustration of the proposed chemical structures of the CDs. Supplementary information is available. See DOI.

Acknowledgments

This work was financially supported by National Research Foundation of Ukraine (project 2025.07/0098), Ministry of Education and Science of Ukraine (project 26BP07-03).

References

1. Z. Alam, S. A. Khan, *Jabirian J. Biointerface Res. Pharm. Appl. Chem.*, 2026, **3**(1), 1-7, DOI: https://doi.org/10.55559/jjbrpac.v3i1.623
2. P. B. Tchounwou, C. G. Yedjou, A. K. Patlolla and D. J. Sutton, *Int. J. Environ. Res. Public Health*, 2012, **9**, 133-164, DOI: 10.1007/978-3-7643-8340-4_6.
3. L. M. Gaetke and C. K. Chow, *Toxicology*, 2003, **189**, 147-163, DOI: 10.1016/S0300-483X(03)00159-8.
4. R. J. Ward, F. A. Zucca, J. H. Duyn, R. R. Crichton and L. Zecca, *Lancet Neurol.*, 2014, **13**, 1045-1060, DOI: 10.1016/S1474-4422(14)70117-6.
5. J. R. Macairan, T. V. de Medeiros, M. Gazzetto, F. Y. Villanueva, A. Cannizzo, R. Naccache, J. Colloid Interface Sci., 2022, **606,** 67-76, DOI: https://doi.org/10.1016/j.jcis.2021.07.156.
6. A. B. Lansdown, *Adv. Pharmacol. Sci.*, **2010**, 910686, DOI: 10.1155/2010/910686.
7. R. J. McDonald, J. S. McDonald, D. F. Kallmes *et al.*, *Radiology*, 2015, **275**, 772-782, DOI: 10.1148/radiol.15150025.
8. D. A. Skoog, F. J. Holler and S. R. Crouch, *Principles of Instrumental Analysis*, Cengage Learning, Belmont, CA, 2007.
9. J. Wang, *Electroanalysis*, 2005, **17**, 1341-1346, DOI: 10.1002/elan.200403270.
10. H. Shabbir, T. Tokarski, D. Ungor, M. Wojnicki, *Materials,* 2021, **14**(24), 7604, DOI: https://doi.org/10.3390/ma14247604
11. M. Shahbaz, U. Salma, M. Z. Alam, M. A. Mujeeb, R. U. H. Ansari, H. A. Basha et al., *J. Fluoresc.*, 2025, **35**(9), 7451-7474, DOI: https://doi.org/10.1007/s10895-025-04166-5
12. T. Garcia-Millan, J. Ramos-Soriano, M. Ghirardello, X. Liu, C. M. Santi, J. C. Eloi et al., *ACS Appl. Mater. Interfaces*, 2023, **15**(38), 44711-44721, DOI: https://doi.org/10.1021/acsami.3c08200

13. V. Lysenko, H. Kuznietsova, N. Dziubenko, I. Byelinska, A. Zaderko, T. Lysenko, V. Skryshevsky, *BioNanoScience*, 2024, 14(2), 1819-1831. DOI: https://doi.org/10.1007/s12668-024-01415-y
14. Z. Yan, Y. Liu, J. Tan, S. Qu. Chem. Eur. J., 2026, e03605. DOI: https://doi.org/10.1002/chem.202603605S
15. S. Y. Lim, W. Shen and Z. Gao, *Chem. Soc. Rev.*, 2015, **44**, 362-381, DOI: 10.1039/C4CS00269E.
16. S. N. Baker and G. A. Baker, *Angew. Chem., Int. Ed.*, 2010, **49**, 6726-6744, DOI: 10.1002/anie.200906623.
17. H. Li, Z. Kang, Y. Liu and S.-T. Lee, *J. Mater. Chem.*, 2012, **22**, 24230-24253, DOI: 10.1039/C2JM34690G.
18. L. Wang, M. Li, W. Li *et al.*, *ACS Sustainable Chem. Eng.*, 2018, **6**, 12668-12674, DOI: 10.1021/acssuschemeng.8b01625.
19. X. Sheng, S. Li, Y. Zhan *et al.*, *Spectrochim. Acta, Part A*, 2021, **263**, 120136, DOI: 10.1016/j.saa.2021.120136.
20. M. F. Rabea, E. Csapó, M. Wojnicki, *Materials*, 2026, **19**, 1810, DOI: 10.3390/ma19091810.
21. A. Bamrah, H. Singh, S. Singh *et al.*, *Chem. Pap.*, 2022, **76**, 6193-6203, DOI: 10.1007/s11696-022-02307-9.
22. K. M. Omer and M. Sartin, *Opt. Mater.*, 2019, **94**, 330-336, DOI: 10.1016/j.optmat.2019.05.045.
23. H. Shabbir, E. Csapó, M. Wojnicki, *Inorganics,* 2023, **11**(6), 262, DOI: 10.3390/inorganics11060262.
24. S. Lu, Z. Li, X. Fu *et al.*, *Dyes Pigm.*, 2021, **187**, 109126, DOI: 10.1016/j.dyepig.2020.109126.
25. H. Li, J. Zhai and X. Sun, *Langmuir*, 2011, **27**, 4305-4312, DOI: 10.1021/la200052t.
26. J. Stetefeld, S. A. McKenna and T. R. Patel, *Biophys. Rev.*, 2016, **8**, 409-427, DOI: 10.1007/s12551-016-0218-6.
27. B. J. Berne and R. Pecora, *Dynamic Light Scattering*, Dover Publications, New York, 2013.
28. A. Topchylo, K. Paliienko, A. Zaderko *et al.*, *ACS Appl. Nano Mater.*, 2025, **8**, 19453-19463, DOI: 10.1021/acsanm.5c03446.
29. Y. Yang, T. Zou, Z. Wang *et al.*, *Nanomaterials*, 2019, **9**, 738, DOI: 10.3390/nano9050738.
30. M. Batool, H. M. Junaid, S. Tabassum *et al.*, *Crit. Rev. Anal. Chem.*, 2022, **52**, 756-767, DOI: 10.1080/10408347.2020.1824117.
31. F. Noun, E. A. Jury and R. Naccache, *Sensors*, 2021, **21**, 1391, DOI: 10.3390/s21041391.
32. K. D. Collins, *Biophys. J.*, 1997, **72**, 65-76, DOI: 10.1016/S0006-3495(97)78647-8.
33. Y. Marcus, *Ions in Solution and Their Solvation*, Wiley, Chichester, 2015.
34. L. Helm and A. E. Merbach, *Chem. Rev.*, 2005, **105**, 1923-1960, DOI: 10.1021/cr030726o.
35. J. N. Israelachvili, *Intermolecular and Surface Forces*, Academic Press, London, 2011.
36. R. Bisauriya, S. Antonaroli, M. Cabibbo and R. Pizzoferrato, *J. Phys.: Conf. Ser.*, 2023, **2579**, 012001, DOI: 10.1088/1742-6596/2579/1/012001.
37. R. Yi, G. I. N. Waterhouse and S. Lu, *Aggregate*, 2022, **3**, e296, DOI: 10.1002/agt2.296.
38. W. Lv, M. Lin, R. Li *et al.*, *Chin. Chem. Lett.*, 2019, **30**, 1410-1414.
39. N. M. Hoang, N. T. B. Ngoc, P. T. L. Huong *et al.*, *J. Fluoresc.*, 2023, **33**, 1359-1366, DOI: 10.1007/s10895-022-03139-2.
40. H. Liao, Z. Wang, S. Chen *et al.*, *RSC Adv.*, 2015, **5**, 66575-66581, DOI: 10.1039/C5RA09948J.
41. Y. Luo, C. Cui, X. Zhang *et al.*, *Molecules*, 2023, **28**, 1566, DOI: 10.3390/molecules28041566.
42. H. Soni, V. Jain, S. Ballal *et al.*, *Nanomaterials*, 2024, **14**, 1766, DOI: 10.3390/nano14211766.

Funding: Not available.

View Article Online
DOI: 10.1039/D6MA00445H

Declaration of competing interest

The authors declare that they have no known competing financial interests or personal relationships that could have appeared to influence the work reported in this paper.

Data availability

Data will be made available on request.